

# The Raise and Peel Model of a Fluctuating Interface

Jan de Gier,<sup>1</sup> Bernard Nienhuis,<sup>2</sup> Paul A. Pearce,<sup>1</sup> and Vladimir Rittenberg<sup>1, 3</sup>

*Received January 29, 2003; Accepted July 17, 2003*

---

We propose a one-dimensional nonlocal stochastic model of adsorption and desorption depending on one parameter, the adsorption rate. At a special value of this parameter, the model has some interesting features. For example, the spectrum is given by conformal field theory, and the stationary non-equilibrium probability distribution is given by the two-dimensional equilibrium distribution of the ice model with domain wall type boundary conditions. This connection is used to find exact analytic expressions for several quantities of the stochastic model. Vice versa, some understanding of the ice model with domain wall type boundary conditions can be obtained by the study of the stochastic model. At the special point we study several properties of the model, such as the height fluctuations as well as cluster and avalanche distributions. The latter has a long tail which shows that the model exhibits self organized criticality. We also find in the stationary state a special surface phase transition without enhancement and with a crossover exponent  $\phi = 2/3$ . Furthermore, we study the phase diagram of the model as a function of the adsorption rate and find two massive phases and a scale invariant phase where conformal invariance is broken.

---

**KEY WORDS:** Growth models; avalanches; conformal field theory; loop models; alternating sign matrices.

## 1. INTRODUCTION

The structure of growing interfaces is a subject of major interest and a characterization of the various universality classes of critical behavior is an

---

<sup>1</sup> Department of Mathematics and Statistics, University of Melbourne, Parkville, Victoria 3010, Australia; e-mail: jdgier@unimelb.edu.au; p.pearce@ms.unimelb.edu.au

<sup>2</sup> Universiteit van Amsterdam, Valckenierstraat 65, 1018 XE Amsterdam, The Netherlands; e-mail: nienhuis@science.uva.nl

<sup>3</sup> Physikalisches Institut, Bonn University, 53115 Bonn, Germany; e-mail: vladimir@th.physik.uni-bonn.de

open question.<sup>(1)</sup> We present a one-dimensional adsorption-desorption model of a fluctuating interface (see Section 2), which belongs to a new universality class. (Part of the results presented in this paper were announced in ref. 2). In this model, that we call the raise and peel model (RPM), the interface follows Markovian dynamics. The adsorption is local (it “raises” the interface) but in the desorption process, part of the top layer of the interface evaporates (one “peels” the interface). The relaxation rules are such that the desorption process takes place through avalanches which have a long tail in their probability distribution function (PDF). The RPM therefore shows self-organized criticality (SOC).<sup>(3-5)</sup> In Section 2 we compare in detail the RPM with the Abelian sand pile model (ASM) and with other growth models. In this section we also define tiles, terraces and clusters which we will use to characterize the interface.

What makes our model special is that for a fine tuning of the adsorption and desorption rates the model is solvable. Namely, the Hamiltonian, which describes the time evolution of the system, is given by a sector of an XXZ quantum chain.<sup>(6,7)</sup> The spectrum of the Hamiltonian can be obtained using the Bethe Ansatz<sup>(8)</sup> and is given by a  $c = 0$  logarithmic conformal field theory (LCFT)<sup>(9)</sup> ( $c$  is the central charge of the Virasoro algebra). This implies that the dynamic critical exponent  $z = 1$ . The connection between the RPM and LCFT was presented elsewhere.<sup>(7)</sup> LCFT appears also in other domains of physics such as systems with quenched disorder and the quantum Hall effect,<sup>(10)</sup> lattice models with  $N = 2$  supersymmetry<sup>(11)</sup> and possibly string theory.<sup>(12)</sup> Once the proper observables are identified the existence of a LCFT behind the stochastic process allows in principle to find the correlation functions of the stochastic process.

The model is special also for a second reason which will take us into the world of combinatorics. The stationary PDF of the system with open boundary conditions is given in terms of weighted restricted solid-on-solid (RSOS) paths. Since there is no detailed balance in the stochastic process we expect it to describe a state “far away from equilibrium.” A number of mathematical conjectures and theorems will allow us to show that in fact the PDF can be understood as an equilibrium PDF defined on a special two-dimensional grid. It turns out that there exists a conjecture<sup>(6)</sup> (conjecture I) that the properly defined normalization factor of the PDF coincides with the number of vertically symmetric alternating sign matrices.<sup>(13,14)</sup> Alternating sign matrices are an important research topic in combinatorics.<sup>(15)</sup> There is a bijection between vertically symmetric alternating sign matrices and the ice model<sup>(16)</sup> defined on a rectangle with special boundary conditions.<sup>(14)</sup> Another bijection relates the ice model with special boundary conditions to a fully packed loop model (FPLM).<sup>(17-19)</sup> A second conjecture (conjecture II) states that the weight of an RSOS path in the PDF of the

stationary state of our model is given by the number of FPLM configurations with the same topology.<sup>(7, 20)</sup> (In Section 3 we will review these topics). We would like to mention that in combinatorics it takes time to prove conjectures.

The conclusion of this chain of arguments is that the weighted RSOS paths in the expression of the PDF of the stationary state can be understood as a uniform PDF in terms of FPLM configurations for which one can use thermodynamics. We will make use of this possibility in Section 5. Moreover, the connections between the stationary state of our interface model, the ice model with special boundary conditions and alternating sign matrices allows to gain new insights also in the last two topics where there are many open questions<sup>(21, 22)</sup> and few facts are known about correlation functions.<sup>(23, 24)</sup>

“Nice” combinatorial objects (the alternating sign matrices are an example) have the magic property that various quantities have simple product expressions. Looking at a few cases one can conjecture exact expressions. The number of alternating sign matrices was such an example<sup>(15)</sup> which took some time to be proved. In the next sections several conjectures will be presented and we will study their physical relevance.

In Section 4 we give a conjecture (conjecture III) for the average size of the terraces and study numerically the size dependence of the average height and width of the interface.

Section 5 contains a recent conjecture (conjecture IV) about the probability to have  $k$  clusters in the stationary state for a system of size  $L$ . We introduce a fugacity  $\zeta$  associated to  $k$  and study the thermodynamic potential of the ensemble of clusters. The thermodynamic potential shows the correct convexity properties, which is a test for the correctness of the conjecture. Moreover, one obtains a phase transition from a phase with a zero density of clusters (small values of  $\zeta$ ) to a phase with a finite density of clusters (large values of  $\zeta$ ). The phase transition takes place when the fugacity is equal to 1. This implies that one has a special surface phase transition<sup>(25)</sup> without needing an enhancement ( $\zeta > 1$ ) for the number of clusters. To our knowledge this phenomenon was not seen for other systems.<sup>(26–28)</sup> One also finds a crossover exponent<sup>(25)</sup>  $\phi = 2/3$ . Since the endpoints of clusters are given by what are usually called contacts, from the value of  $\phi$  we determine the critical exponent related to the contact-contact two-point function.

In Section 6 we study the production of avalanches in our model. We give a conjecture (conjecture V) for the probabilities to have an adsorption or a desorption event for different system sizes. We also study numerically the moments of the PDF for desorption processes with different tile numbers (avalanche sizes). We show that for large systems the PDF has

a divergent dispersion i.e., the PDF shows a long tail. This shows that our model is in the SOC class.

Section 7 deals with the RPM when one changes the value of the ratio of the adsorption and desorption rates away from 1. No analytical methods are known for this new situation. We therefore have numerically diagonalized the Hamiltonian and used finite size scaling in order to understand the phase structure.

Lastly, in Section 8, we present our conclusions in which we try to convince the reader that in spite of the fact that the model was not inspired by a particular physical phenomenon, it has many remarkable properties bringing together different aspects of physics and mathematics.

## 2. THE MODEL

We consider an interface of a one-dimensional lattice of size  $L+1$  ( $L=2n$ ). The non-negative heights  $h_i$  obey the restricted solid-on-solid (RSOS) rules,

$$h_{i+1} - h_i = \pm 1, \quad h_0 = h_L = 0, \quad h_i \geq 0. \quad (1)$$

Alternatively, one can describe the interface using slope variables  $s_i = (h_{i+1} - h_{i-1})/2$ , ( $i = 1, \dots, L-1$ ). In order to characterize the interface, we give some useful definitions. A segment of a configuration with endpoints at the sites  $a$  and  $b$  is defined by the conditions:  $h_a = h_b = h$  and  $h_j > h$  for  $a < j < b$ . If  $h = 0$ , the segment is called a cluster. A terrace is an interval where the slopes are zero for all the sites.

There are  $C_n = (2n)! / ((n+1)(n!)^2)$  possible configurations of the interface. In Fig. 1 we show a configuration for  $n = 8$ , ( $L = 16$ ). This configuration has two clusters, a terrace of length one separating the two clusters, one terrace of length one at the peak of the first cluster and a terrace of length five inside the second cluster.

The dynamics of the interface is described in a transparent way in the language of tiles (tilted squares) which cover the area between the interface

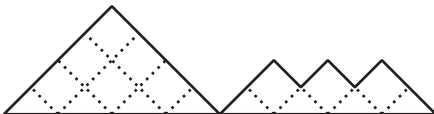


Fig. 1. A configuration of the interface with two clusters.

and the substrate ( $h_{2i} = 0, h_{2i+1} = 1, (i = 0, \dots, n)$ ). There are six tiles in the first cluster in Fig. 1 and three in the second.

We consider the interface as separating a film of tiles deposited on the substrate, from a rarefied gas of tiles. We are interested to find the evolution of the interface toward the stationary state and to study the properties of the interface in this state.

The evolution of the system in discrete time (Monte-Carlo steps) is given by the following rules. With a probability  $P_i = 1/(L-1)$  a tile from the gas hits the site  $i, (i = 1, \dots, L-1)$ . Depending on the value of the slope  $s_i$  at the site  $i$ , the following processes can occur:

- (i)  $s_i = 0$  and  $h_i > h_{i-1}$ . The tile hits a local peak and is reflected.
- (ii)  $s_i = 0$  and  $h_i < h_{i-1}$ . The tile hits a local minimum. With a probability  $u_a$  the tile is adsorbed ( $h_i \mapsto h_i + 2$ ) and with a probability  $1 - u_a$  the tile is reflected.
- (iii)  $s_i = 1$ . With probability  $u_d$  the tile is reflected after triggering the desorption of a layer of tiles from the segment  $h_{i+b} = h_i$ , i.e.,  $h_j \mapsto h_j - 2$  for  $j = i+1, \dots, i+b-1$ . This layer contains  $b-1$  tiles. With a probability  $1 - u_d$ , the tile is reflected and no desorption takes place.
- (iv)  $s_i = -1$ . With probability  $u_d$  the tile is reflected after triggering the desorption of a layer of tiles belonging to the segment  $h_{i-b} = h_i$ , i.e.,  $h_j \mapsto h_j - 2$  for  $j = i-b+1, \dots, i-1$ . With a probability  $1 - u_d$  the tile is reflected and no desorption takes place.

In our model the adsorption, which occurs on terraces, is local but the desorption is not. To illustrate how the desorption takes place, we show in Fig. 2 the layer of tiles which is desorbed after a tile has hit the site 1, there are 5 tiles desorbed. The same tiles are desorbed if the incoming tile would have hit site 7. Desorption takes place within one cluster. We notice that the number of tiles removed through desorption (this number is always odd) can be of the order of the system size  $L$  and therefore one can conclude that in our model the desorption takes place through avalanches.

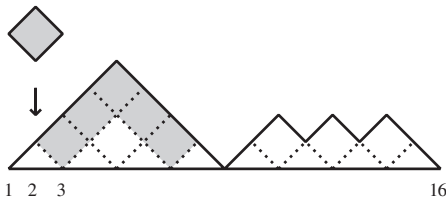


Fig. 2. A desorption event. The incoming tile at site 1 triggers an avalanche of 5 tiles, which are shaded. All of the shaded tiles are removed in the desorption event.

Before discussing the physics of the model, we give the rates for the continuous time evolution of the interface. At the local minima of the interface, adsorption ( $h_i \mapsto h_i + 2$ ) takes place with a rate  $u = u_a/u_d$ . Desorption of a segment  $h_a = h_b$ , i.e.,  $h_j \mapsto h_j - 2$  for  $a < j < b$ , takes place with a rate,

$$\delta(s_a - 1) + \delta(s_b + 1). \quad (2)$$

The rate  $u$  is the single free parameter in the model.

The Hamiltonian  $H$  which gives the time evolution in the vector space of RSOS configurations, has matrix elements  $H_{cd} = -r_{cd}$ , where  $r_{cd}$  are the rates for the transitions  $d \rightarrow c$  given above ( $\sum_c H_{cd} = 0$ ). The unnormalized probability  $P_c(t)$  to find the system in the configuration  $c$  at time  $t$  is given by the imaginary time Schrödinger equation,

$$\frac{d}{dt} P_c(t) = -\sum_d H_{cd} P_d(t). \quad (3)$$

Since  $H$  is an intensity matrix, it has a zero eigenvalue with a trivial bra and a nontrivial ket which gives the probabilities in the stationary state,

$$\begin{aligned} \langle 0| H = 0, & \quad \langle 0| = (1, 1, \dots, 1), \\ H |0\rangle = 0, & \quad |0\rangle = \sum_c P_c |c\rangle, \quad P_c = \lim_{t \rightarrow \infty} P_c(t). \end{aligned} \quad (4)$$

In most of this paper we will consider  $u = 1$ , Section 7 being an exception.

As we are going to show in Section 6, our model for  $u = 1$  is of the SOC class (self-organized criticality). We here anticipate some results and compare the present model with the Abelian sandpile model (ASM) of Bak, Tang and Wiesenfeld<sup>(3)</sup> which is a paradigm for SOC:

(i) In the stationary state of the RPM the balance is obtained when the number of tiles adsorbed on the film of tiles on the substrate is equal to the number of tiles desorbed. In the ASM the balance is obtained when the number of grains of sand adsorbed on the film of sand is equal to number of grains that leave the film through the boundary.

(ii) The heights in the RPM can be of the order of the system size (see Section 4) therefore the RPM can also be viewed as a growth model. The heights are finite in ASM.

(iii) The RSOS paths of the RPM correspond to the recurrent configurations of the ASM. While through toppling one configuration of ASM is taken into one other configuration only, in the RPM one configuration

can go, with different probabilities, into several configurations. One should add that in the ASM, topplings give a simple physical interpretation for the avalanches. There is not yet a simple physical mechanism for desorption transitions in the RPM.

(iv) The ASM is not critical in  $d = 1$ ,<sup>(29)</sup> but it is in  $d = 2$ .<sup>(30)</sup> In both dimensions the stationary probability distribution is uniform in the space of recurrent states. The  $d = 1$  RPM is critical, the stationary probability distribution in RPM is not uniform in the space of RSOS paths (see Section 3).

(v) The  $2+1$  (2 space, 1 time) dimensional ASM has a dynamic exponent  $z = 2$ <sup>(31,32)</sup> and the stationary 2-d probability distribution describes a critical system with correlation functions given by a  $c = -2$  LCFT. At  $u = 1$  the  $1+1$  RPM has a dynamic exponent  $z = 1$  and the spectrum of the Hamiltonian is given by generic characters of a  $c = 0$  LCFT. The nonuniform stationary probability distribution in the space of RSOS paths can be obtained by making a correspondence to the 2-d ice model with special boundary conditions (see Section 3). What is therefore common to the two models is that the stationary probability distributions which describe phenomena “far away from equilibrium” are given by 2-d equilibrium systems.

(vi) Avalanches can be studied if one perturbs the system near the stationary state. For the ASM the average size of the avalanche diverges with the size of the system, whereas it stays finite for the RPM. This is true for at least a large range of values of the parameter  $u$ . The explanation is simple. We denote by  $P_a$  the probability to have adsorption and by  $P_d$  the probability to have desorption and take into account that one adsorbs only one tile. The average number of tiles desorbed is,

$$\langle T \rangle = \frac{P_a}{P_d}, \quad (5)$$

which is finite unless  $P_d$  vanishes as  $L \rightarrow \infty$ . At  $u = 1$  the probability distribution function for an avalanche of a certain size has an algebraic fall-off implying that one has relatively large probabilities to produce large avalanches (see Section 6). This is typical for SOC.

Since the RPM is also a model for interface growth it is interesting to compare it with other models of this kind. For example in the Rouse model of polymer dynamics,<sup>(33)</sup> adsorption (desorption) takes place at the local minima (maxima) with the same rate. One has detailed balance,  $z = 2$  and the stationary state is given by a uniform PDF of RSOS paths. This is

a PDF for a directed polymer model (DPM), for which the average height  $\langle \bar{h} \rangle$  increases like  $L^{1/2}$ .<sup>(34)</sup> A modification of the Rouse model by Koduvely and Dhar<sup>(35)</sup> has local rates and detailed balance but includes also adsorption (desorption) rates depending on the next nearest neighbor heights. In this model one finds an increased value of  $z$  ( $z \approx 2.5$ ), the average height and the width being of the order of  $L^{1/2}$ . As we are going to see, in the RPM we do not have detailed balance, locality is lost, and at least for  $u = 1$  one has  $z = 1$  and the heights and widths increase logarithmically with the size of the system.

### 3. RSOS, LOOP, AND SIX-VERTEX CORRESPONDENCE

In this section we make the connection between our model and the dense  $O(1)$  or Temperley–Lieb loop model,<sup>(36,37)</sup> and we review the conjectured relation of the stationary state to a model of fully packed loops on a rectangle. This connection enables us to interpret the non-equilibrium stationary state as an equilibrium PDF.

Each RSOS path of the RPM corresponds to a “boundary diagram” of loops<sup>(38)</sup> in the following way. On each RSOS path, draw the equal height contour lines, as in Fig. 3a. By straightening out the surface, keeping the contour lines and rotating the picture around the horizontal axis, we obtain Fig. 3b. The contour lines connect pairs of sites and Fig. 3b thus defines a link pattern (boundary diagram).

The RPM was inspired<sup>(2)</sup> by a stochastic model on the link patterns, called the dense  $O(1)$  or Temperley–Lieb loop model (TLLM). Namely, for  $u = 1$  the Hamiltonian of the RPM can be rewritten as

$$H = \sum_{j=1}^{L-1} (1 - e_j), \quad (6)$$

where the  $e_j$  satisfy the Temperley–Lieb relations

$$e_j^2 = (q + q^{-1}) e_j, \quad e_j e_{j \pm 1} e_j = e_j, \quad e_j e_k = e_k e_j \quad \text{for } |j - k| > 1, \quad (7)$$

with  $q = \exp(i\pi/3)$ . We remark here that the  $e_j$  admit a representation in terms of Pauli spin matrices. In that representation, the Hamiltonian (6)



Fig. 3. An interface with contour lines and the corresponding link pattern.



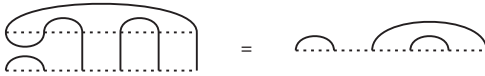
becomes that of the quantum XXZ spin chain with diagonal boundaries.<sup>(39)</sup> This model is integrable and quantities such as the conformal scaling exponents can be calculated exactly, for example using Bethe Ansatz techniques.<sup>(8)</sup>

The  $e_j$  can be pictorially represented by,

$$e_j = \left[ \begin{array}{c} \text{---} \\ | \quad \cdot \quad \cdot \quad \cdot \quad | \\ \text{---} \end{array} \right] \begin{array}{c} \text{---} \\ \cup \\ \cap \\ \text{---} \end{array} \left[ \begin{array}{c} \text{---} \\ | \quad \cdot \quad \cdot \quad \cdot \quad | \\ \text{---} \end{array} \right] \begin{array}{c} \text{---} \\ | \\ \text{---} \end{array} \quad (8)$$


1    2             $j-1$      $j$      $j+1$      $j+2$      $L-1$      $L$

The action of  $e_j$  on a link pattern of contour lines is given by placing the graph of  $e_j$  underneath that of the link pattern and removing the closed loops and the intermediate dashed line. They allow one to remove closed loops and contract links in composite pictures. The action of  $e_1$  on one of the link patterns for  $L=6$  (corresponding to a desorption event) is for example given by,



$$\text{---} \quad (9)$$

As an example we calculate the Hamiltonian for  $L=6$  on the five basis states,



$$\quad (10)$$

and we find,

$$H = - \begin{pmatrix} -2 & 2 & 2 & 0 & 2 \\ 1 & -3 & 0 & 1 & 0 \\ 1 & 0 & -3 & 1 & 0 \\ 0 & 1 & 1 & -3 & 2 \\ 0 & 0 & 0 & 1 & -4 \end{pmatrix} \quad (11)$$

In the basis (10) the stationary state  $|0\rangle$  of  $H$  is given by

$$|0\rangle = (11, 5, 5, 4, 1). \quad (12)$$

Here we have chosen the smallest element to equal 1. Using the definitions in (4) we therefore find the normalization factor to be  $\langle 0|0\rangle = 26$ . Below we show that the normalization acquires an extra meaning from an enumeration problem.

The RPM model for  $u = 1$  is thus equivalent to the Temperley–Lieb loop (TLLM) model. For the TLLM the surprising observation was made<sup>(6)</sup> that the normalization of the stationary state is equal to the partition function of an equilibrium statistical mechanics system (conjecture I). This observation has deeper consequences which we will now briefly review.

For this purpose we consider a six-vertex model on a  $(L-1) \times L/2$  rectangle with boundary conditions such that the arrows on the sides all point inward and those on the bottom boundary all point outward (domain wall boundary conditions<sup>(40)</sup>). The arrows on the top boundary alternate, see for example Fig. 4. The six-vertex configurations are in one to one correspondence with horizontally symmetric alternating sign matrices<sup>(13, 14)</sup> and can also be reformulated as configurations of a fully packed loop model (FPLM)<sup>(17–19)</sup>.

The six-vertex configurations on the square lattice can be transformed into fully packed loop (FPL) configurations. FPL configurations are configurations of paths such that every site is visited by exactly one path. We divide the square lattice into its even and odd sub-lattice denoted by A and B respectively. Instead of arrows, only those edges are drawn that on sub-lattice A point inward and on sub-lattice B point outward, see Fig. 5.

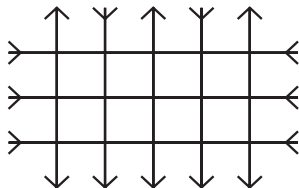


Fig. 4. A  $5 \times 3$  rectangle with domain wall boundary conditions on the left, right and bottom boundary and alternating arrows at the top boundary.

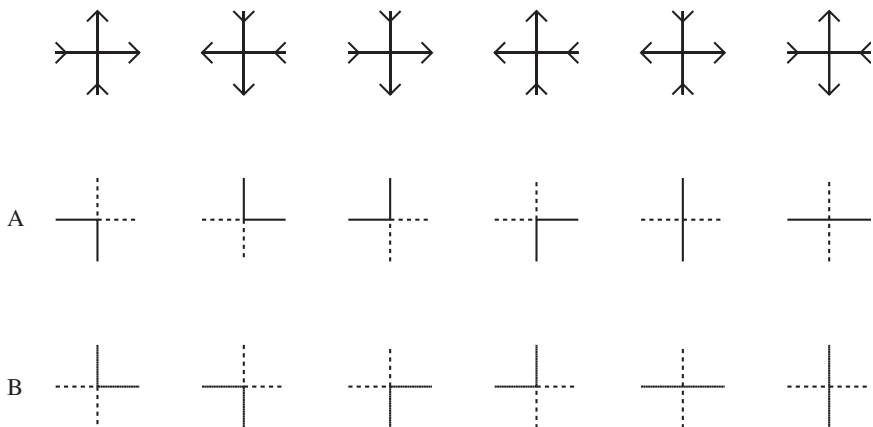


Fig. 5. FPL vertices on sub-lattices A and B derived from the six arrow vertices.

We take the vertex in the upper left corner to belong to sub-lattice A. The special six-vertex boundary condition translates into a boundary condition for the loops. Paths either form closed loops, or begin and end on boundary sites which are prescribed by the boundary in- and out-arrows on sub-lattice A and B respectively. In this way it can be seen that the six-vertex configurations on the rectangle in Fig. 4 are in one to one correspondence with FPL configurations on the grid in Fig. 6, see also Appendix A.

The paths that start and end on boundary sites (we disregard the closed loops in the bulk) define a link pattern in the same way as did the Temperley–Lieb loops. There is an interesting connection between the coefficients of the stationary state of the Hamiltonian of our model at  $u = 1$ , or equivalently the Hamiltonian as given by (6), and the enumeration

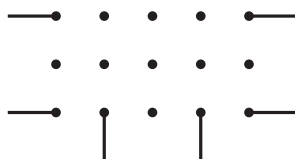


Fig. 6. FPL grid corresponding to Fig. 4

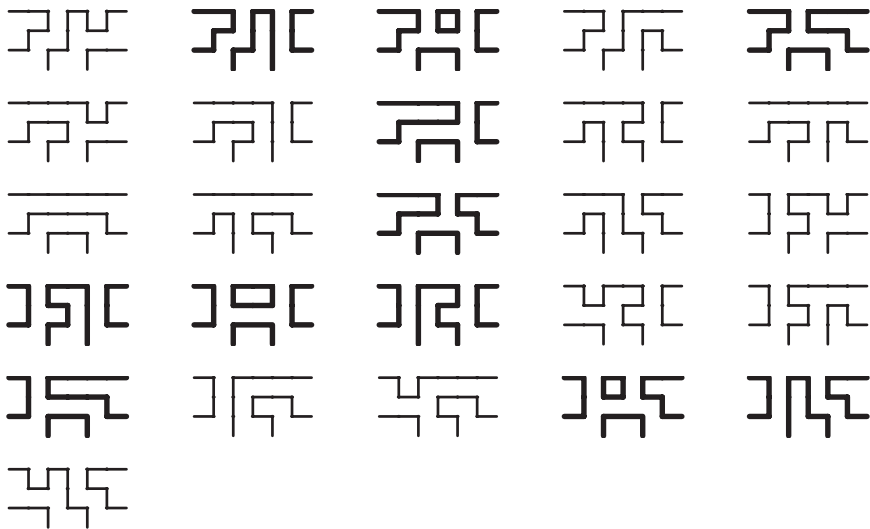


Fig. 7. The 26 FPL diagrams for  $L = 6$ . The 11 diagrams corresponding to link pattern 1 in (10) are printed bold.

of FPL configurations on the rectangular grid: the link patterns in the stationary state of the TLLM and those in the FPLM appear with the same probability<sup>(7,20)</sup> (conjecture II). Take for example the stationary state for  $L = 6$  given by (12). The FPL configurations on the  $5 \times 3$  rectangle are shown in Fig. 7. Their total number is 26, which is the sum of the integers in (12), and they can be categorized according to the five link patterns given in (10). One finds that the number of diagrams corresponding to link pattern 1 is 11 (these are printed bold in Fig. 7), to link pattern 2 is 5, to link pattern 3 is 5, to link pattern 4 is 4 and to link pattern 5 is 1.

We have just illustrated for  $L = 6$  the connection between the coefficients of the stationary state of the TLLM written in the basis of link patterns and the number of configurations of the FPLM with that same link pattern. The connection between the stationary state and this enumeration problem has many consequences. For example, on a conceptual level, one understands a stationary state “far from equilibrium” as an equilibrium PDF. Also, the scaling properties of the RPM and the critical properties of the FPLM are related to the scaling dimensions of an LCFT. Furthermore, exact results obtained by studying the properties of the enumeration problem can be used to calculate stationary correlation functions and expectation values.

The number of six-vertex configurations on a  $(L+1) \times (L+1)$  square with domain wall boundary conditions that are invariant under reflection in the horizontal symmetry axis is equal to that of the  $(L-1) \times L/2$  rectangle with the special boundary condition, see Fig. 4. The total number of such configurations is known and is equal to the number of  $(L+1) \times (L+1)$  horizontally symmetric alternating sign matrices (in existing literature more commonly denoted as vertically symmetric alternating sign matrices) which is given by,<sup>(14)</sup>

$$A_{2n+1}^V = \prod_{j=0}^{n-1} (3j+2) \frac{(2j+1)! (6j+3)!}{(4j+2)! (4j+3)!}, \quad L = 2n. \quad (13)$$

The leading asymptotic terms of  $A_{2n+1}^V$  are given by

$$\begin{aligned} \ln A_{L+1}^V &= s_0(L-1) L/2 + \left( s_0 - \frac{1}{2} \ln 2 \right) (L-1) \\ &\quad - \frac{5}{144} \ln L^2 + O(1), \quad s_0 = \ln \frac{3\sqrt{3}}{4}, \end{aligned} \quad (14)$$

where  $s_0$  is the entropy per site. The first term in (14) is proportional to the area of the rectangle. In Appendix A we show that the second term in (14) is a surface contribution coming from the top boundary, and not from the other sides of the rectangle. This observation is important for the understanding of Section 5. The surface contribution turns out to be related to a string expectation value.

#### 4. TERRACES AND HEIGHTS IN THE STATIONARY STATE

We now consider, from the point of view of growth models, various quantities which characterize the interface in the stationary state. In this section we look at the terraces and heights and in the next section we will consider clusters. This separation is due to the fact that there exists a conjecture for the cluster PDF and we will be able to study in detail the properties of the ensemble of clusters. In Section 6 we will consider the same interface from the point of view of SOC.

One can make<sup>(43)</sup> a conjecture (conjecture III) for the fraction of the interface covered by terraces for a system of size  $L$ ,

$$\tau_L = \frac{1}{L-1} \sum_{j=1}^{L-1} \langle 1 - |s_j| \rangle = \frac{3L^2 - 2L + 2}{(L-1)(4L+2)}. \quad (15)$$

This conjecture was verified up to  $L = 18$ . Eq. (15) implies that for large  $L$ , three quarters of the interface is covered with terraces. On a terrace, half of the sites correspond to local minima where adsorption can occur and one half to local maxima where only reflections can occur. Desorption cannot occur on terraces. This allows us to make an estimate of the ratio of the probabilities to have adsorption respectively desorption: asymptotically  $P_a/P_d = 3/2$ . This relation is obtained in a different way in Section 6 from another conjecture. The fact that the results coincide is reassuring.

The average height  $\langle \bar{h} \rangle$  and interface width  $w$ , which characterizes the roughness of the surface in the stationary state, have the following definitions,

$$\bar{h}^m = \frac{1}{L} \sum_{i=1}^L [h_i/2]^m, \quad w = \sqrt{\langle \bar{h}^2 - \bar{h}^2 \rangle}, \quad (16)$$

Obviously  $\bar{h} = 0$  for the substrate.

We analyzed the behavior of the heights using exact data up to  $L = 18$ . For  $L = 18$  the average height has only the value  $\langle \bar{h} \rangle \approx 0.28$ , which implies that the average height increases very slowly with the size of the system. We therefore assumed the following behavior,

$$\langle \bar{h} \rangle = a \ln L + b, \quad (17)$$

and solved for  $a$  and  $b$  for data points corresponding to  $L-2$  and  $L$ . The results for successive pairs of data points are given in Table I. The fact that the values of  $a$  and  $b$  do not change much suggests that indeed (17) may be correct. In Fig. 8 we plot the values of  $\langle \bar{h} \rangle$  as a function of  $\ln L$  together with the fit (17) using the values for  $L = 18$  of Table I. We obtained less convincing data when fitting the heights to power laws.

**Table I. Heights**

$L$	$a$	$b$
6	0.126477	-0.092001
8	0.128676	-0.095941
10	0.129859	-0.098400
12	0.130643	-0.100206
14	0.131225	-0.101653
16	0.131686	-0.102870
18	0.132067	-0.103924

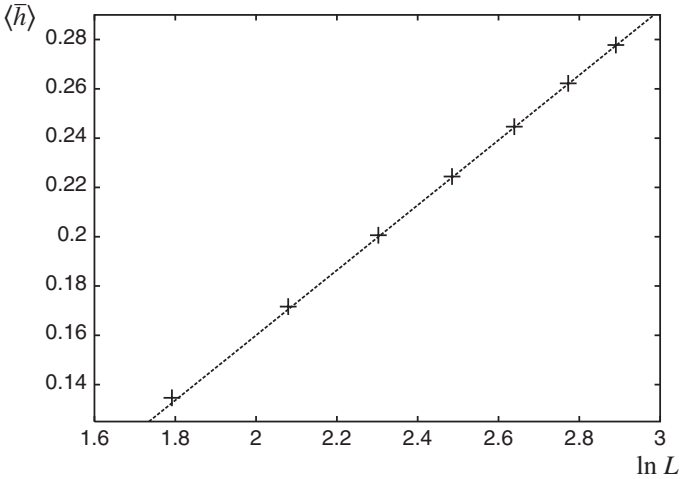


Fig. 8. The  $L$  dependence of the average height for  $L = 6, 8, \dots, 18$ . The curve is given by  $\langle \bar{h} \rangle = 0.132 \ln L - 0.104$ .

Doing a similar analysis for the widths we find that our data are compatible with,

$$w \sim (\ln L)^{0.35(5)}. \quad (18)$$

Because of the logs the formulae given in (17) and (18) are probably not the last word. What is certain is that the height and the width grow slowly with the size of the system implying that the surface is only marginally rough. H. Hinrichsen and L. Sittler<sup>(44)</sup> used Monte Carlo simulations for our model to obtain the Family–Vicsek<sup>(45)</sup> scaling function for large lattices, finding,

$$\exp(w(L, t)^2) \sim L^\gamma f(t/L), \quad \gamma = 0.192 \pm 0.010. \quad (19)$$

They confirm in this way that  $z = 1$  and that the width increases logarithmically with  $L$  as in (18). They also found that in the stationary state  $w^2$  stays of the order of 1 when  $L$  varies between 16 and 65536.

It is interesting to mention that marginally rough surfaces (with  $z = 1.581$  corresponding to the directed percolation universality class) were also encountered<sup>(46, 47)</sup> at a critical point dividing a moving rough KPZ phase from a smooth, massive phase.

## 5. THE ENSEMBLE OF CLUSTERS IN THE STATIONARY STATE

An obvious geometric observable to characterize a configuration of the interface is the set of sites  $j$  ( $j$  even) for which  $h_j = 0$  (the sites 0 and  $L$  always belong to this set). These sites are also called contact points. This set is for example important to study the desorption, since two consecutive points in this set are the endpoints of a cluster and as discussed in Section 2 desorption takes place within one cluster only. For this set one can define various correlation functions. Here we will be mainly interested in the number of clusters which is defined by

$$k = \sum_{r=1}^n \delta(h_{2r}). \quad (20)$$

As explained in Section 3, to each interface, or each RSOS path, corresponds a set of FPL diagrams. The clusters in the RSOS paths can be easily identified in the FPL diagrams and we will take (20) also as a definition of the clusters on FPL diagrams. The set of contact points in the interface where  $h_j = 0$  maps to a corresponding set on FPL paths, see e.g., Fig. 9.

We consider the partition function

$$Z_n^{\text{FPL}}(\zeta) = \sum_{\text{FPL cfigs.}} \zeta^k, \quad (21)$$

where the summation is over FPL configurations on the  $(L-1) \times L/2$  rectangular grid ( $L = 2n$ ), see Section 3, and  $\zeta = e^\mu$  where  $\mu$  is a chemical potential (or a magnetic field). Because of the RSOS-FPL connection, the two dimensional partition function  $Z_n^{\text{FPL}}(\zeta)$  can also be computed in terms of weighted RSOS paths. It is interesting to notice that the partition function  $Z_n^{\text{DPM}}(\zeta)$  for unweighted RSOS path corresponding to the stationary

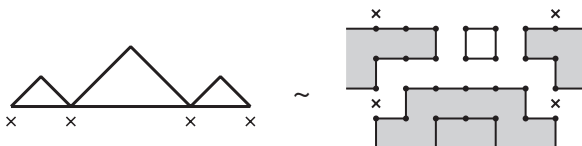


Fig. 9. An interface for  $L = 8$ . The contact points 0, 2, 6, and 8 are denoted by  $\times$ . One of the corresponding FPL diagrams, with the same contact points, is shown on the right. The three clusters it contains are shaded.



state of the Rouse model (RM)<sup>(33)</sup> is known<sup>(48)</sup> and it was used to describe the surface critical behavior in the directed polymer model (DPM). To see the effect of weighted RSOS paths we will compare our results in the following to those obtained in the DPM.

Let us define  $P_n(k)$  as the probability to have  $k$  clusters for a system of size  $L = 2n$ . The partition function (21) can then be written as

$$Z_n^{\text{FPL}}(\zeta) = \mathcal{P}_n(\zeta) A_{2n+1}^{\text{V}}, \quad (22)$$

where  $A_{2n+1}^{\text{V}}$  is given by (13) and

$$\mathcal{P}_n(\zeta) = \sum_{k=1}^n P_n(k) \zeta^k, \quad \mathcal{P}_n(1) = 1. \quad (23)$$

The thermodynamic potential is given for large  $n$  by,

$$\Omega^{\text{FPL}}(\zeta, n) = -\ln Z_n^{\text{FPL}}(\zeta) = \Omega(\zeta, n) - \ln A_{2n+1}^{\text{V}}. \quad (24)$$

The leading asymptotics of the last term in (24) are given in (14), and do not affect the critical properties of the ensemble of clusters. The average number of clusters, its second moment and the pressure can be derived from  $\Omega(\zeta, n)$  via,

$$\langle k \rangle = -\zeta \frac{\partial}{\partial \zeta} \Omega(\zeta, n), \quad (25)$$

$$\langle k^2 \rangle - \langle k \rangle^2 = -\left( \zeta \frac{\partial}{\partial \zeta} \right)^2 \Omega(\zeta, n), \quad (26)$$

$$p = -\frac{1}{2n} \Omega(\zeta, n), \quad (27)$$

In order to compute the thermodynamic potential, one needs the expression for  $P_n(k)$ . There is a conjecture for this expression<sup>(49)</sup> (checked up to  $L = 18$ ) and its proof is an open combinatorial problem. Let us mention that some time ago the expression of  $A_{2n+1}^{\text{V}}$  was also a conjecture which was subsequently proved. In the present paper we will accept the conjecture for  $P_n(k)$  and study its consequences for the physics of the ensemble of clusters. This study will give an indirect confirmation of the conjecture since convexity properties of the thermodynamic potential are satisfied.

### 5.1. A Conjecture for $P_n(k)$

In ref. 49 the following conjecture (conjecture IV) for  $P_n(k)$  was made,

$$P_n(k) = k \frac{4^{n+k} (1/2)_{n+k}}{27^n (1/3)_{2n}} \frac{(3n+2)! (2n-k-1)!}{n! (n-k)! (2n+k+1)!}, \quad (28)$$

where we have used the Pochhammer symbol  $(a)_n = \Gamma(a+n)/\Gamma(a)$ . The partition function (23) can now be rewritten as,

$$\mathcal{P}_n(\zeta) = A_n \zeta F_n(\zeta), \quad (29)$$

where,

$$A_n = \frac{2^{2n-1} (1/2)_n}{27^n (1/3)_{2n}} \frac{(3n+1)!}{n!(n+1)! (2n-1)!}, \quad (30)$$

$$F_n(\zeta) = {}_3F_2 \left( \begin{matrix} 2, 1-n, n+3/2 \\ 2-2n, 3+2n \end{matrix}; 4\zeta \right). \quad (31)$$

Here we have used the definition (see, e.g., ref. 50) of the hypergeometric function

$${}_3F_2 \left( \begin{matrix} a_1, a_2, a_3 \\ b_1, b_2 \end{matrix}; \zeta \right) = \sum_{k=1}^{\infty} \frac{(a_1)_k (a_2)_k (a_3)_k}{(b_1)_k (b_2)_k k!} \zeta^k. \quad (32)$$

Using Eqs. (25) and (29) we get,

$$\langle k \rangle = 1 + \zeta \frac{F'_n(\zeta)}{F_n(\zeta)}. \quad (33)$$

### 5.2. The Thermodynamic Potential of the Ensemble of Clusters

To derive thermodynamic potential we have to find the asymptotics of  $F_n$ . This can be achieved by starting with the hypergeometric equation (see, e.g., ref. 50) satisfied by  $F_n$ ,

$$D(D+1-2n)(D+2+2n) F_n(\zeta) = 4\zeta(D+2)(D+1-n)(D+3/2+n) F_n(\zeta), \quad (34)$$

where  $D = \zeta d/d\zeta$ . We will need to distinguish the cases  $\zeta < 1$  and  $\zeta > 1$ .

•  $\zeta < 1$ . For small  $\zeta$  we expect  $F_n$  to grow as a polynomial in  $n$ . Keeping only the terms with coefficients proportional to  $n^2$  in (34) we get

$$F'_n(\zeta) = \frac{2}{1-\zeta} F_n(\zeta). \quad (35)$$

It is clear that our assumption on  $F_n$  is consistent with (35) for  $\zeta < 1$ . Using (33) we find for the average number of clusters,

$$\langle k \rangle = \frac{1+\zeta}{1-\zeta} \quad (\zeta < 1). \quad (36)$$

•  $\zeta > 1$ . For large  $\zeta$  the main contributions will come from terms proportional to  $\zeta^n$  and thus  $F'_n \sim nF_n$ . From Eqs. (33) and (34) we can derive the following equation for  $\langle k \rangle$  in the limit  $n \rightarrow \infty$ ,

$$(4\zeta - 1)(D^2\langle k \rangle + 3(\langle k \rangle - 1)D\langle k \rangle + (\langle k \rangle - 1)^3) = 4n^2(\zeta - 1)(\langle k \rangle - 1), \quad (37)$$

which has the following solution

$$\langle k \rangle = \sqrt{\frac{\zeta - 1}{4\zeta - 1}} L \quad (\zeta > 1). \quad (38)$$

Comparing the expressions (36) and (38) for the number of clusters, one notices that the density of clusters  $\rho = \langle k \rangle / L$  vanishes for  $\zeta < 1$  as  $L \rightarrow \infty$  (one has few large clusters) and stays finite for  $\zeta > 1$  (one has many small clusters). This implies that  $\zeta = 1$  is the critical point of a special surface transition.<sup>(25)</sup> It is interesting to note that for the DPM the critical value of the fugacity is  $\zeta_c = 2$  and not  $\zeta_c = 1$  as in our model. The reason is simple: the critical point marks the appearance of a finite density of clusters. This is realized more easily for the weighted RSOS paths where the configurations with many clusters have the largest probabilities. For a uniform distribution of RSOS configurations, as in the DPM, one has to further increase the value of the fugacity to reach the critical point. This phenomenon is the rule rather than the exception, the special transition is the result of the enhancement obtained taking  $\zeta > 1$ . This can be seen in the  $O(n)$  model ( $-2 \leq n < 1$ )<sup>(26-28)</sup> or at the collapse transition at the  $\Theta$  point.<sup>(51-53)</sup> The fact that in the RPM one is already at the special transition point ( $\zeta_c = 1$ ) is probably a result of the special role played by the boundaries in our model (see Section 3).

Let us also observe, see (36) and (38), that for  $\zeta < 1$  as well as  $\zeta > 1$ , the number of clusters increases with the fugacity. This is what one expects

if the conjecture (28) is correct. From (27) the pressure can be calculated for  $\zeta > 1$  as a function of  $\rho$ . We find,

$$p = \ln \left( \frac{1-\rho}{1+\rho} \sqrt{\frac{1+2\rho}{1-2\rho}} \right) \approx 2\rho^3(1+3\rho^2+O(\rho^3)). \quad (39)$$

This is an increasing function of  $\rho$  which is yet another indication of the validity of the conjecture. Notice also that for small densities the pressure is not proportional to  $\rho$  but to  $\rho^3$ .

### 5.3. The Cluster Ensemble at Criticality

The critical behavior at a special transition is governed by a single exponent, the cross-over exponent  $\phi$ .<sup>(25)</sup> We expect,

$$\langle k \rangle \sim \begin{cases} n(\zeta - \zeta_c)^{1/\phi-1} & (\zeta > \zeta_c) \\ n^\phi & (\zeta = \zeta_c). \\ (\zeta_c - \zeta)^{-1} & (\zeta < \zeta_c) \end{cases} \quad (40)$$

Moreover, the exponent of the second moment should be twice that of the first,

$$\langle k^2 \rangle - \langle k \rangle^2 \sim n^{2\phi} \quad (\zeta = \zeta_c). \quad (41)$$

Following Polyakov,<sup>(54)</sup> we expect the following scaling form of the cluster distribution function near the critical point,

$$P_n(k) = \frac{1}{\langle k \rangle} f(k/\langle k \rangle). \quad (42)$$

The large  $x$  behavior of  $f(x)$  is related to the same exponent  $\phi$ ,<sup>(55)</sup>

$$\lim_{x \rightarrow \infty} f(x) \sim x^s e^{-ax^\delta}, \quad \delta = \frac{1}{1-\phi}. \quad (43)$$

The small  $x$  behavior of  $f(x)$  is related to the large  $n$  behavior of the probabilities  $P_n(k)$ ,

$$\lim_{x \rightarrow 0} f(x) = bx^\theta, \quad \lim_{n \rightarrow \infty} P_n(k) = b \frac{k^\theta}{\langle k \rangle^{1+\theta}}. \quad (44)$$

For the DPM<sup>(48)</sup> the scaling function  $f(x)$ <sup>(56)</sup> has the following simple expression,

$$f(x) = \sqrt{\frac{2}{\pi}} x \exp(-x^2/2), \quad (45)$$

from which we read off that  $\phi = 1/2$  and  $\theta = 1$ . In our model the number of clusters, calculated from (38), is equal to,

$$\langle k \rangle = \frac{2n}{\sqrt{3}} \sqrt{\zeta - 1}, \quad (46)$$

from which we get  $\phi = 2/3$  (see Eq. (40)). We have also obtained the average number of clusters for any system size and  $\zeta = 1$ ,

$$\langle k \rangle = \frac{1}{3} \left( \prod_{j=0}^{n-1} \frac{(2j+1)(3j+4)}{(j+1)(6j+1)} - 1 \right). \quad (47)$$

This expression was obtained by showing that it satisfies the same recursion relation and initial conditions as its defining equation,

$$\langle k \rangle = \sum_{k=1}^n k P_n(k), \quad (48)$$

with (28) substituted for  $P_n(k)$ . Using (48) one can derive (47) by using an algorithm from Zeilberger which is conveniently implemented in a Mathematica package by Paule and Schorn.<sup>(57)</sup> The result (47) was tested in Monte Carlo simulations up to system size  $n = 2048$ . From (47) we obtain the large  $n$  behavior of  $\langle k \rangle$ ,

$$\langle k \rangle \approx \frac{\Gamma(1/3) \sqrt{3}}{2\pi} (2n)^{2/3} \quad (n \rightarrow \infty), \quad (49)$$

in agreement with the second relation in (40). The last of the relations of (40) is a consequence of (36). The fact that all the scaling relations (40) are satisfied should not be taken for granted since our calculations are based on the conjecture (28).

For the fluctuations of the cluster distribution we found numerically,

$$\langle k^2 \rangle - \langle k \rangle^2 \approx 0.659(1) L^{4/3} - 0.73(1) L^{2/3}. \quad (50)$$

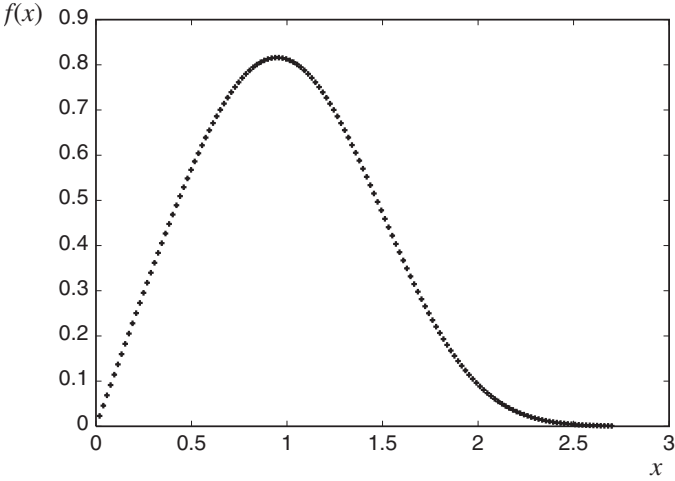


Fig. 10. The scaling function  $f(x)$  obtained for  $L = 600$ .

The small  $x$  behavior of the scaling function (42) can be determined using (44) and we find,

$$f(x) \approx 3 \left( \frac{\Gamma(1/3) \sqrt{3}}{2\pi} \right)^3 x, \quad (51)$$

which implies  $\theta = 1$ . Finally we have determined numerically from the conjecture (28) the scaling function (42), see Fig. 10.

#### 5.4. $\phi = 2/3$ and Conformal Invariance

For isotropic systems (for DPM this is not the case), and for surface transitions which occur through enhancement, the crossover exponent is related to the bulk and surface scaling dimensions, <sup>(25, 27)</sup>

$$\phi = (1 - \Delta_s) \nu = \frac{1 - \Delta_s}{2(1 - \Delta_b)}, \quad (52)$$

The exponent  $\Delta_s$  is related to the two-point contact correlation function exponent on the boundary of the halfplane. The bulk correlation length exponent  $\nu$  enters in the expression of  $\phi$  because of standard finite size scaling arguments (one uses (41)). Eq. (52) can be used for the  $O(n)$  model ( $-2 \leq n < 1$ ) and one obtains  $\phi = 1/2$  since  $\Delta_s = \Delta_b$ , <sup>(27)</sup> or for the collapse transition at the  $\Theta$  point where one obtains  $\phi = 8/21$  <sup>(52, 53)</sup> since  $\Delta_b = 1/8$  and  $\Delta_s = 1/3$ . <sup>(59, 58)</sup>

In our model, the susceptibility given by (50) (see also (41)) is related to the two-point contact correlation in a halfplane. This can be understood by looking at Fig. 9. The two sides of the rectangle can be aligned with the bottom edge in a larger horizontal segment which for large  $L$  becomes the line which borders the halfplane. This gives the factor  $1 - \Delta_s$  in (52). What is more obscure in the case of the RPM, is the finite size scaling factor  $\nu$ . In our case there is no enhancement factor and no simple way to take the system away from criticality in order to define  $\nu$ . If we choose to ignore  $\nu$  we have

$$\phi = 1 - \Delta_s, \quad (53)$$

from which we derive  $\Delta_s = 1/3$  which is one of the known surface scaling dimensions.<sup>(60)</sup>

## 6. AVALANCHES

In the last sections we have considered properties of the stationary state. Here we are going to study the response of the system to small perturbations around the stationary state. We are therefore going to investigate the production of avalanches and show that our model exhibits SOC.

In order to study avalanches we consider the following processes in discrete time (see Section 2). In the stationary state let a tile from the rarefied gas fall on the site  $i$  with probability  $p_i = 1/(L-1)$  and count how many tiles  $T$  are released in the process. This number is zero if the tile is reflected,  $-1$  if it is adsorbed and is a positive odd number if the falling tile triggers desorption. Repeating the process many times we can measure the probability  $R(T, L)$  to observe  $T$  tiles for a system of size  $L$ . This PDF can be computed from the known transition rates and the conjectured probability distributions of RSOS configurations.

Studying systems of different sizes  $L$ , we were led to the following conjecture (conjecture V) for the probability  $P_a(L) = R(-1, L)$  to have an adsorption process and  $P_d(L) = 1 - R(-1, L) - R(0, L)$  to have a desorption process,

$$P_a(L) = \frac{3L(L-2)}{4(2L+1)(L-1)}, \quad P_d(L) = \frac{L-2}{L-1} - 2P_a(L). \quad (54)$$

This conjecture was checked up to  $L = 18$ . The fact that one is able to obtain simple expressions for properties of the system away from equilibrium is remarkable since it suggests that the methods used to prove some of the conjectures for alternating sign matrices could be extended to time dependent properties.

Using the expressions for  $P_a(L)$  and  $P_d(L)$  we conclude that in the large  $L$  limit the average number of tiles  $\langle T \rangle$  observed in desorption increases to a maximum value of  $3/2$ . This implies that, on average, there are few tiles desorbed. We remind the reader that in Section 4 using a completely different argument we obtained the same asymptotic value for  $\langle T \rangle$ . In order to analyze the properties of the avalanches, it is convenient to write  $T = 2v - 1$ , ( $v = 1, 2, \dots$ ) and to consider  $v$  as the size of the avalanche. Given the occurrence of an avalanche, its size  $v$  is distributed according to the PDF,

$$S(v, L) = \frac{R(2v-1, L)}{P_d(L)}. \quad (55)$$

If the PDF of tiles presents a long tail, i.e., if one has SOC, finite size scaling theory (FSS)<sup>(4)</sup> suggests the following form for this PDF,

$$S(v, L) = v^{-\tau} F(v/L^D). \quad (56)$$

One way to get the exponents of the FSS function is to consider the moments,<sup>(61)</sup>

$$\langle v^m \rangle = \sum_{v=1} v^m S(v, L) \approx A(m) L^{\sigma(m)}, \quad (57)$$

for which one expects,

$$\sigma(m) = \begin{cases} 0, & m < \tau - 1 \\ D(m + 1 - \tau), & m > \tau - 1 \end{cases}. \quad (58)$$

**Table II. Avalanche Exponents  $\sigma(m)$**

$L \setminus m$	3	4	5
6	1.31250	2.81250	5.81250
8	1.14050	2.42898	4.59306
10	1.05707	2.25429	4.06439
12	1.00985	2.15976	3.78047
14	0.98066	2.10312	3.60721
16	0.96159	2.06682	3.49219
18	0.94867	2.04244	3.41113
$\infty$	0.91830	1.98162	3.02038



Since  $\langle T \rangle = 3/2$ , one has  $\sigma(1) = 0$  and  $A(1) = 5/4$ . In order to compute the moments, we have used the exact values of  $S(v, L)$  for  $L$  up to 18 and VBS approximants.<sup>(62)</sup> For  $m = 1.5$  one obtains  $\sigma(1.5) = 0$  with  $A(1.5) \approx 1.745$ . For  $m = 2$ ,  $\sigma(2)$  is hard to determine suggesting that the dispersion (second moment) diverges logarithmically. In Table II we give the estimates and extrapolations for the exponents  $\sigma_L(3)$ ,  $\sigma_L(4)$ , and  $\sigma_L(5)$ , where

$$\sigma_L(m) = L \frac{\langle v^m \rangle_L - \langle v^m \rangle_{L-1}}{\langle v^m \rangle_{L-1}}. \quad (59)$$

These results suggest that  $\sigma(m) = m - 2$  for  $m \geq 2$  (with logarithmic corrections close to  $m = 2$ ). If this is indeed the case we conclude that  $D = 1$  and  $\tau = 3$ . Because of crossover effects one cannot preclude small changes in the values of these two exponents. The value  $D = 1$  was to be expected since  $L$  is the single characteristic length in our system. A consistency check was done assuming  $D = 1$  in (56) to see for which value of  $\tau$  one finds a data collapse for the scaling function  $F(v/L)$ . Since we have data up to  $L = 18$  only we cannot expect a precise value neither of  $\tau$  nor of  $F$ . Nevertheless as shown in Fig. 11, a data collapse is visible for  $\tau = 3.2$ , in agreement with the value  $\tau = 3$  mentioned earlier. We conclude that the PDF of tiles shows long tail and that therefore our model is in the SOC class.

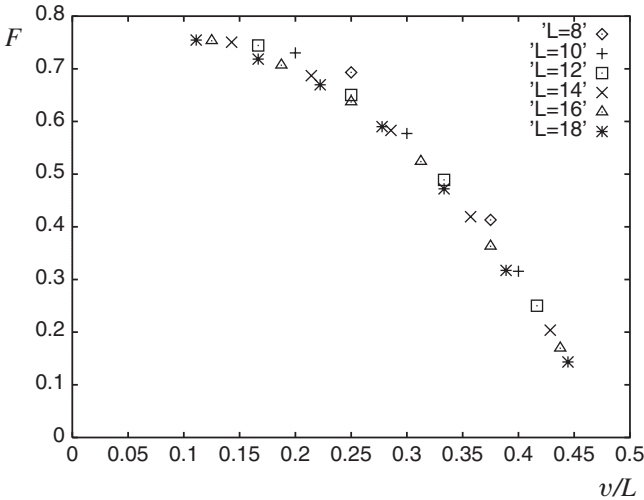


Fig. 11. Avalanche scaling function  $F(v/L)$ . The data are obtained for  $v > 1$  and  $L = 8, \dots, 18$ .

## 7. THE INTERFACE MODEL AWAY FROM THE TEMPERLEY–LIEB RATES

In this section we study the interface model described in Section 2 for adsorption rates  $u$  different from 1. This study is interesting not only because we expect the physics to be different but also from a theoretical point of view. Changing the value of  $u$ , one perturbs the LCFT in a non-local way and it is not clear what is the nature of the phases one obtains. In principle one can obtain phases that are scale invariant but not conformally invariant. Such a scenario was not yet seen, as far as we know, in other physical systems.

Let us forget for a moment that we know what happens at  $u = 1$ . We will try to reason what might occur for general  $u$  using physical considerations. One has to keep in mind that the RSOS paths are confined to a triangle and this geometry might have consequences for the phase structure. At  $u = 0$  the system is not critical. The stationary state (energy zero) corresponds to the substrate and the first degenerate excited energy level corresponds to having a tile on top of the substrate. This energy (energy gap) is equal to 2 (corresponding to the rate given by Eq. (2)), and is  $L - 1$  times degenerate since the tile can be desorbed from  $L - 1$  sites. No avalanches are produced in the substrate.

If one slightly increases  $u$  the energy gap also changes slightly (in fact it decreases), the degeneracy of the first level is lifted and the first Brillouin zone appears. This is the massive phase I of the model. In this phase one expects the stationary interface to be composed mainly of terraces, the average height  $\langle \bar{h} \rangle$  and the density of clusters should stay finite in the thermodynamic limit. The interface is smooth in this phase and the avalanche distribution should not show a long tail.

Increasing the value of  $u$  over a critical value  $u_{c,1}$  the density of clusters should vanish and  $\langle \bar{h} \rangle$  should increase algebraically in  $L$ , the interface being rough. We expect this phase to be massless and the probability distribution of the avalanches to show a long tail, therefore we will call this phase the SOC phase. Invoking what we know about the physics at  $u = 1$  where the interface is marginally rough, one might argue  $u_{c,1} = 1$ .

If  $u$  becomes larger than a critical value  $u_{c,2}$  one expects a second massive phase that we denote by II. Let us explain why. It is useful to consider instead of  $u$  its inverse  $w = 1/u$  as a variable and to take  $w < 1$ . We redefine the time scale such that one has a rate 1 for adsorption and  $w$  for desorption. At  $w = 0$ , the only RSOS path entering the stationary state is the one corresponding to the edges of the triangle of height  $L/2$ . In this configuration there is one cluster which contains the maximum number of tiles and  $\langle \bar{h} \rangle = (L - 2)/8$ . Like for  $u = 0$ , for  $w = 0$  we do not have

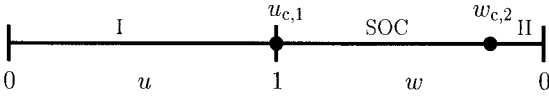


Fig. 12. Expected phase diagram

avalanches, this time because we do not have desorption. The first excited state which corresponds to the configuration with one tile less than in the stationary state, has an energy equal to 1 (corresponding to the adsorption rate) and is degenerate. It turns out that the spectrum of the Hamiltonian (including degeneracies!) at  $w = 0$  is identical up to a factor  $1/2$  to the spectrum of the Hamiltonian at  $u = 0$ . This observation deserves a more detailed explanation which we are not going to give here. For small values of  $w$ , the  $L - 1$  degeneracy of the first energy level is lifted giving rise to the first Brillouin zone. Increasing the value of  $w$  we span the massive phase II up to a critical value  $w_{c,2} = 1/u_{c,2}$ . In this phase,  $\langle \bar{h} \rangle$  is of the order  $L$  and the density of clusters is zero.

To sum up, according to this scenario, illustrated in Fig. 12, one expects two massive phases, one massless phase and two critical points  $u_{c,1}$  and  $u_{c,2}$ .

To check this scenario we have limited ourselves to finite size scaling studies (FSS) to find out when a system is gapless and to determine the dynamic scaling exponent  $z$ . Unfortunately analytical methods can be used for  $u = 1$  only. We have diagonalized numerically the Hamiltonian up to  $L = 16$  and have determined  $E_1(u, L)$  and  $E_2(u, L)$ , the energies of the first and second excited states as functions of  $u$  and  $L$  (or of  $w$  and  $L$ ). From our experience, when dealing with nonlocal Hamiltonians, FSS methods have some times convergence problems and can be efficient in some cases and not in others.

At  $u = 1$  it is known<sup>(2)</sup> that,

$$LE_1(1, L) = 2\pi v + o(1), \quad LE_2(1, L) = 3\pi v + o(1), \quad (60)$$

where the sound velocity  $v = 3\sqrt{3}/2$ . We will first assume that, like for  $u = 1$ , in the whole SOC phase the dynamic exponent  $z = 1$ . In Figs. 13 and 14 we have plotted the values of  $LE_1(u, L)$  respectively  $LE_1(w, L)$  for various number of sites. If one would have a single critical point at  $u = w = 1$  (this is not our scenario) one would expect crossings for values of  $u$  and  $w$  close to 1. The values of  $u$  and  $w$  for which one obtains crossings for various lattice sizes should converge to 1 for large  $L$ . This is not at all what one sees. We notice that there are two crossings at 0.5 and 0.85 in the  $u$  domain. The second crossing might well converge to 1. There are also

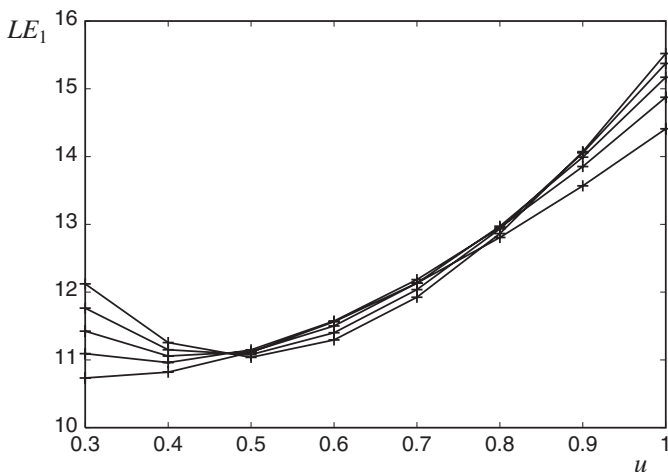


Fig. 13. Scaled  $E_1$  as a function of the adsorption rate  $u$  for  $L=8, 10, 12, 14,$  and  $16$  (the smaller systems give smaller values for  $u=1$ ). The curves are a guide to the eye only.

two crossings in the  $w$  domain, at 0.02 and 0.13. The data suggest, as expected two massive phases, one for  $u < 0.5$  and another one for  $w < 0.02$ . What happens in between is less clear. Taking into account that we only have results for small systems, all we could do were some consistency checks.

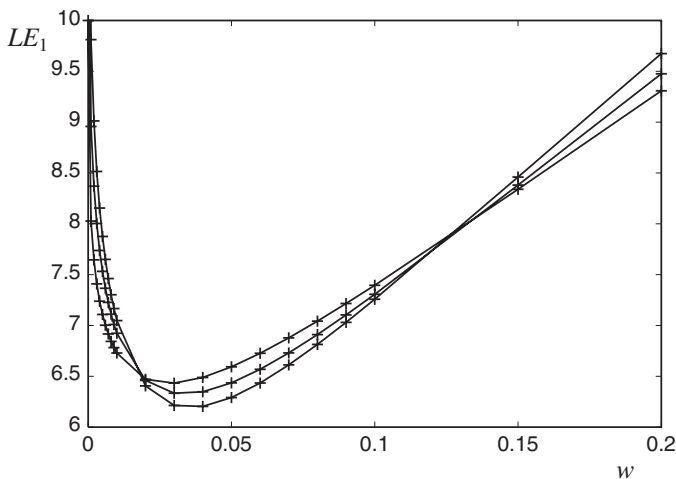


Fig. 14. Scaled  $E_1$  as a function of the adsorption rate  $w$  for  $L=10, 12,$  and  $14$  (the smaller systems give smaller values for  $w=0.2$ ). The curves are a guide to the eye only.

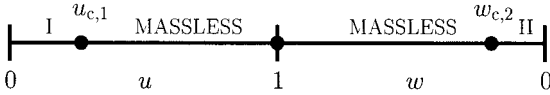


Fig. 15. Proposed phase diagram.

One possibility is that in the whole domain  $u > 0.5$ ,  $w > 0.02$  one has a massless phase with  $z = 1$ . To investigate this possibility we have checked using different extrapolation methods if for a given value of  $u$  (respectively  $w$ ) the quantities  $LE_1(u, L)$  converge for large  $L$ . For  $u > 0.7$  and  $w$  close to 1 the data are compatible with a massless phase with  $z = 1$ , although the convergence is less clean than for  $u = 1$  (the extrapolated values are far away from the value for  $L = 16$ ). However, from the numerics we cannot exclude the possibility that we only have  $z = 1$  at  $u = 1$  and a different value, albeit very close to 1, elsewhere. In the remaining domain it is hard to make any clear statement because of convergence problems. This picture invalidates already part of our scenario since  $u = 1$  is in the middle of a massless phase and thus cannot correspond to  $u_{c,1}$ . If that is the case, the phase diagram of Fig. 12 should be replaced by Fig. 15.

Can we conclude that in the domain where we have  $z \approx 1$  we also have LCFT? This possibility can be easily checked looking at the ratio  $E_2(u, L)/E_1(u, L)$  for large values of  $L$ . The reason we are looking at this ratio is the following one. Because of the universality of the amplitudes in LCFT, see (60) where now the sound velocity  $v$  can be a function of  $u$ , this ratio should have the value  $3/2$  independent of  $u$  in the whole domain of the SOC phase. In a massless phase which is not described by a LCFT this ratio can have any value (no universality). On the other hand, in the massive phases this ratio should be equal to 1 since the second energy level belongs to the same Brillouin zone as the first energy level.

In Table III we give the values of the ratios for different values of  $u$  and  $L$  as well as (when possible) the extrapolated values for large  $L$ . One

Table III. Ratio  $E_2/E_1$ 

$L \setminus u$	0.01	0.3	0.9	1.0	1.111	1000
8	1.068015	1.422562	1.419503	1.390377	1.355468	
10	1.057506	1.442180	1.462111	1.425500	1.381065	1.11059
12	1.047632	1.439921	1.488372	1.446044	1.393992	1.11237
14	1.039483	1.427343	1.506046	1.459091	1.400681	1.11164
16	1.032983	1.409821	1.518746	1.467896		
$\infty$	1.00691	–	1.629253	1.500120	1.415755	–

notices that, as expected, for  $u = 1$  one gets the value  $3/2$ . For  $u = 0.01$  (in the first massive phase) the extrapolated value is, as expected 1. For  $u = 0.3$  (also expected to be in the massive phase I, the ratio first increases with  $L$  and then decreases, probably toward the value 1. In the second massive phase ( $u = 1000$ ), the values of the ratios first increase (from  $L = 10$  to  $L = 12$ ) and then decrease (from  $L = 12$  to  $L = 14$ ). This makes any extrapolation procedure meaningless and for this reason we didn't give a value for  $L = \infty$  in Table III. Nevertheless, one can see that for  $u = 1000$ , the three values of the ratio are close to 1 (the expected value). These observations provide a supplementary check for the existence of the two massive phases.

We now come to the most interesting result of our analysis. For  $u = 0.9$  and  $1.111$ , assumed to be in the SOC phase, the ratios do not converge to the value 1.5. This implies that although one is scale invariant ( $z$  close to 1) one is not conformally invariant.

To conclude, although based only on limited FSS studies, our results suggest that changing the value of the rates from their Temperley–Lieb values gives a phase diagram with two massive phases and a massless phase with a nontrivial structure. There is one point ( $u = 1$ ) described by a LCFT and around this point one has a domain, of a size which is not well known, where one stays scale invariant but one doesn't have LCFT. Hopefully Monte-Carlo simulations will clarify this picture.

## 8. CONCLUSIONS

The Hamiltonian of the Temperley–Lieb loop model (TLLM) defined in the space of link patterns for  $q = \exp(i\pi/3)$  (see Eq. (7)) is an intensity matrix giving the time evolution of a stochastic process. As shown in ref. 60 its spectrum is given by the characters of a  $c = 0$  LCFT. The same Hamiltonian corresponds to a sector of the XXZ quantum chain with quantum group boundary conditions.<sup>(39)</sup> The first motivation in our study was to see the specific features of a stochastic model in which one has LCFT. Mapping the link patterns into RSOS configurations (see Section 3) we get a model of a fluctuating interface: the raise and peel model (RPM) described in Section 2 for  $u = 1$ . The main observation is that this model is simple and that the study of its physics is very interesting. This was a pleasant surprise. The physics is not so transparent for other stochastic models related to extensions of the TLLM.<sup>(7, 63)</sup>

A particular feature of the RPM is that the PDF which gives the stationary distribution of the RSOS configurations can be understood in terms of an enumeration of fully packed loop (FPL) configurations on a rectangle for which one side plays a different role than the other three. This

is one of the conjectures<sup>(7,20)</sup> on which this paper is based. Accepting this conjecture which was checked for small system sizes, one concludes that the “far away from equilibrium” stationary state of the one-dimensional RPM is in fact a two-dimensional equilibrium distribution.

This is not the end of the story. The FPL configurations can be mapped into the ice model on a rectangle with domain wall boundary conditions on three edges and alternating arrows on the fourth (see Section 3). The boundary conditions induce highly nonlocal effects in the bulk. One effect of the boundary conditions is that one has phase separation.<sup>(21)</sup> It is not obvious to see such a phase separation if one looks at the RSOS interface.

The various aspects of ice model with special boundary conditions are related to the “The many faces of alternating-sign matrices”<sup>(22)</sup> to which, we think that the RPM has added a useful new one. For example, the RPM model allows for easy Monte-Carlo simulations in order to obtain correlation functions, which are much harder to get for the other “faces” of the alternating sign matrices.

We now sum up the main results we have obtained about the physical properties of the RPM for  $u = 1$ . In Section 4 we show that the average height and width of the interface increase logarithmically with the system size indicating that the interface is only marginally rough,  $3/4$  of the interface being covered by terraces.

Based on a conjecture for the expression of the probability to have  $k$  clusters ( $k+1$  contacts of the interface with the horizontal line)<sup>(49)</sup> for a system of size  $L$  and introducing a fugacity (enhancement parameter)  $\zeta$  related to the number of contacts, we have derived in Section 5 the interface tension as a function of  $\zeta$ . An important result of this paper is that there is a special surface transition at  $\zeta = 1$ , separating a phase ( $\zeta < 1$ ) with a finite number of clusters (density zero) from a phase ( $\zeta > 1$ ) with a finite density of clusters. This implies that no enhancement ( $\zeta > 1$ ) is needed to obtain the special surface transition.<sup>(25)</sup> This fact which is certainly related to the unusual role of the boundaries in the FPL model, is interesting for two reasons. Firstly we are not aware of any model in which one obtains a special transition without enhancement. Secondly, the RPM is related to the dense  $O(1)$  model ( $q = \exp(i\pi/3)$  in Eq. (7)). The common lore<sup>(27)</sup> is that the ordinary  $O(n)$  model can have a special transition with a finite enhancement for  $-2 \leq n < 1$  only. We not only have the surface transition but we get it without enhancement. Various scaling laws have been checked and the crossover exponent  $\phi = 2/3$  was obtained. This exponent also gives the large  $L$  behavior of the susceptibility related to the two-point contacts correlation function. This correlation can be obtained for example by using Monte-Carlo simulations in the RPM. It would be much more difficult to obtain it directly in the FPLM.

In Section 6 we have studied the SOC properties of the RPM showing that the avalanches of tiles produced by desorption have a PDF which, for large systems sizes, has a finite average (as opposed to sand pile models) but a divergent dispersion.

In Section 7 we have studied the RPM for  $u$  different from 1. No connections with FPLM or with integrable systems are known in this case. For small and very large values of  $u$  the system is massive. Finite size scaling studies suggest that around  $u = 1$  the dynamic scaling exponent  $z$  has a value closed to 1 (for  $u = 1$  one has  $z = 1$ ) but that conformal invariance is lost. Such a scenario was not seen in other models.

The list of open questions which should start with the possible physical applications of the model is too long to be written. Progress in combinatorics (to prove the conjectures) and efforts to obtain analytic expressions for the correlation functions are obviously required. We assume that the first results which will push forward the understanding of the model will come from Monte-Carlo simulations.

## APPENDIX A. PHYSICAL INTERPRETATION OF THE ASYMPTOTICS OF $A_{2n+1}^V$

We now show that the surface contribution to the asymptotics of  $A_{2n+1}^V$ , given in (14), has the interpretation of a probability. To see that we compare (14) to the asymptotics<sup>(64)</sup> of the number  $A_{L+1}^{(65, 66)}$  of six-vertex configurations on the  $(L+1) \times (L+1)$  square with domain wall boundary conditions. This expression does not contain a surface term,

$$\ln A_{L+1} = s_0(L+1)^2 - \frac{5}{72} \ln L^2 + O(1). \quad (61)$$

We stress that a surface term does appear when one considers weighted configurations of the six-vertex model.<sup>(21)</sup>

To understand the meaning of the surface contribution in (14) we use the FPLM. Requiring horizontal symmetry for FPL diagrams on a square implies that a loop segment runs along the horizontal symmetry axis and also that the left and right boundary layers are fixed, see Fig. 16. The number  $A_{L+1}^V$  thus counts all FPL diagrams on the lower (or upper) rectangle of the right hand side picture of Fig. 16.

The probability that the horizontal symmetry axis of an arbitrary FPL diagram on the square is covered by a loop segment can now be easily calculated. Using (14) and (61) we find,

$$\frac{(A_{2n+1}^V)^2}{A_{2n+1}} \sim \left( \frac{1}{2} e^{-s_0} \right)^{2n} \quad (n \rightarrow \infty), \quad (62)$$



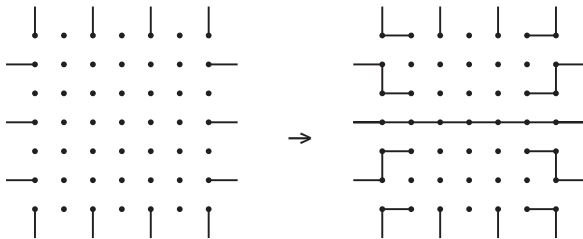


Fig. 16. Fixed edges for horizontally symmetric FPL diagrams.

where  $s_0$  is the entropy per site given in (14). Note that (62) is a product of probabilities in which the value  $1/2$  is screened by a factor  $e^{-s_0}$  due to bulk effects. The probability in (62) can be interpreted as a string expectation value (see, e.g., ref. 67).

The surface contribution in (14) therefore has the interpretation of a probability. It arises due to the boundary with the alternating arrows in Fig. 4, and not from the domain wall boundaries on the sides and bottom. The fact that the leading behaviour in (62) is purely exponential and does not contain an algebraic factor is very surprising for the following reason. The probability that the first edge of the horizontal symmetry axis is drawn is known as a particular case of the refined alternating sign matrix conjecture<sup>(41)</sup> which meanwhile is proved.<sup>(24, 42)</sup> We denote this probability by  $p_1$  and it is given by,

$$\binom{3n-1}{n-1} \frac{(3n+1)! (4n+1)!}{(n+1)! (6n+1)!} \approx \sqrt{\frac{2}{3\pi n}}, \quad (63)$$

which is algebraic. In the probability (62) that the entire horizontal symmetry axis contains a loop segment, the algebraic dependence has disappeared and is transformed into a screening factor of  $e^{-s_0}$  per edge. A further amusing point is that for  $n = 1$ , (62) gives an estimate of 0.2798... for the entropy per site which is already very close to its exact value  $s_0 = 0.2616\dots$

## ACKNOWLEDGMENTS

This research is supported by the Australian Research Council, and by the Foundation “Fundamenteel Onderzoek der Materie” (FOM). VR is an ARC IREX Fellow. We thank H. Hinrichsen and A. Owczarek for discussions.

## REFERENCES

1. Some recent reviews are A.-L. Barabasi and H. E. Stanley, *Fractal Concepts in Surface Growth* (Cambridge University Press, 1995); E. H. Hinrichsen, *Adv. Phys.* **49**:815 (2000).
2. J. de Gier, B. Nienhuis, P. A. Pearce, and V. Rittenberg, *Phys. Rev. E* **67**:016101 (2002).
3. P. Bak, C. Tang, and K. Wiesenfeld, *Phys. Rev. Lett.* **59**:381 (1987); *J. Phys. A* **38**:364 (1988).
4. Some recent reviews are H. J. Jensen, *Self Organised Criticality* (Cambridge University Press, 1998); D. Dhar, *Physica A* **264**:1 (1999).
5. A. Ben-Hur and O. Biham, *Phys. Rev. E* **53**:R1317 (1996); A. Vespignani and S. Zapperi, *Phys. Rev. E* **57**:6345 (1998).
6. M. T. Batchelor, J. de Gier, and B. Nienhuis, *J. Phys. A* **34**:L265 (2001).
7. P. A. Pearce, V. Rittenberg, J. de Gier, and B. Nienhuis, *J. Phys. A* **35**:L661 (2002).
8. F. C. Alcaraz, M. N. Barber, M. T. Batchelor, R. J. Baxter, and G. R. W. Quispel, *J. Phys. A* **20**:6397 (1987).
9. I. I. Kogan and A. Nichols, hep-th/0203207 (2002) and references therein; M. Flohr, hep-th/0111228 (2001); M. R. Gaberdiel, hep-th/0111260 (2001); S. Kawai, hep-th/0204169 (2002).
10. V. Gurarie and A. W. W. Ludwig, *J. Phys. A* **35**:L3771 (1999); I. I. Kogan and A. M. Tsvelik, *Mod. Phys. Lett. A* **15**:931 (2000).
11. K. Schoutens, P. Fendley, and J. de Boer, *Phys. Rev. Lett.* **90**:120402 (2003).
12. I. I. Kogan and D. Polyakov, *Int. J. Mod. Phys. A* **16**:2559 (2001).
13. D. P. Robbins, math.CO/0008045 (2000).
14. G. Kuperberg, *Ann. Math.* **156**:835 (2002).
15. D. M. Bressoud, *Proofs and Confirmations: The story of the Alternating Sign Matrix Conjecture* (Cambridge, Cambridge University Press, 1999)
16. E. Lieb, *Phys. Rev. Lett.* **18**:692 (1967).
17. N. Elkies, G. Kuperberg, M. Larsen, and J. Propp, *J. Algebraic Combin.* **1**:111–132/219–234 (1992).
18. M. T. Batchelor, H. W. J. Blöte, B. Nienhuis, and C. M. Yung, *J. Phys. A* **29**:L399 (1996).
19. B. Wieland, *Electron. J. Combin.* **7**, research paper 37 (2000).
20. A. V. Razumov and Yu. G. Stroganov, math.CO/0104216 (2001), cond-mat/0108103 (2001).
21. P. Zinn-Justin, *Phys. Rev. E* **62** (2000), 341; V. Korepin and P. Zinn-Justin, *J. Phys. A* **33** (2000), 7053; P. Zinn-Justin, cond-mat/0205192 (2002).
22. J. Propp, *Discr. Math. and Theor. Comp. Sci. Proc. AA* **43** (2001).
23. N. M. Bogoliubov, A. G. Pronko, and M. B. Zvonarev, *J. Phys. A* **35**:5525 (2002).
24. Yu. G. Stroganov, math-ph/0204042 (2002).
25. K. Binder, in *Phase Transitions and Critical Phenomena*, Vol. 8, C. Domb and J. L. Lebowitz, eds. (Academic Press, London, 1983), p. 2.
26. R. Balian and G. Toulouse, *Ann. Phys.* **83**:28 (1973).
27. T. W. Burkhardt, E. Eisenriegler, and I. Guim, *Nucl. Phys. B* **316**:559 (1989).
28. S. L. A. Queiroz, *J. Phys. A* **27**:L363 (1995).
29. P. Ruelle, private communication.
30. S. Mathieu and P. Ruelle, *Phys. Rev. E* **64**:066130 (2001); P. Ruelle, *Phys. Lett. B* **539**:172 (2002) and references therein.
31. E. V. Ivashkevich and V. B. Priezhev, *Physica A* **254**:97 (1998).
32. D. Dhar, *Physica A* **263**:4 (1999).
33. P. E. Rouse, *J. Chem. Phys.* **21**:1272 (1953).

34. V. Privman and N. M. Svrakic, *Directed Models of Polymers, Interfaces, and Clusters: Scaling and Finite Size Properties*, Lecture Notes in Physics, Vol. 38 (Springer Verlag, Berlin Heidelberg, 1989).
35. H. N. Koduvely and D. Dhar, *J. Stat. Phys.* **90**:57 (1998).
36. V. Pasquier, *Nucl. Phys. B* **285**, 162 (1987); *J. Phys. A* **20**, L1229 (1987); *J. Phys. A* **20**, 5707 (1987).
37. A. Owczarek and R. J. Baxter, *J. Stat. Phys.* **49**:1093 (1987).
38. P. P. Martin, *Potts Models and Related Problems in Statistical Mechanics* (World Scientific Singapore, 1991).
39. V. Pasquier and H. Saleur, *Nucl. Phys. B* **330**:523 (1990).
40. V. E. Korepin, *Comm. Math. Phys.* **86**:391 (1982).
41. W. H. Mills, D. P. Robbins, and H. Rumsey, *Invent. Math.* **66**:73 (1982); W. H. Mills, D. P. Robbins, and H. Rumsey, *J. Combin. Theory Ser. A* **34**:340 (1983).
42. D. Zeilberger, *New York J. Math.* **2**:59 (1996).
43. We thank Yu. G. Stroganov for this conjecture.
44. H. Hinrichsen and L. Sittler, private communication.
45. F. Family and E. Vicsek, *J. Phys. A* **18**:L75 (1985); *Dynamics of Fractal Surfaces* (World Scientific Singapore, 1991).
46. U. Alon, M. R. Evans, H. Hinrichsen, and D. Mukamel, *Phys. Rev. E* **57**:4997 (1998).
47. H. Hinrichsen, private communication.
48. R. Brak, J. W. Essam, and A. L. Owczarek, *J. Stat. Phys.* **93**:155 (1998); *J. Stat. Phys.* **102**:997 (2001), and references therein.
49. J. de Gier, math.CO/0211285 (2002).
50. A. Erdélyi, *Higher Transcendental Functions*, Vol. 1, (McGraw-Hill, New York, 1953).
51. P. G. de Gennes, *Scaling Concepts in Polymer Physics* (Cornell University Press, Ithaca, NY, 1979).
52. T. Prellberg and A. L. Owczarek, *J. Phys. A* **27**:1811 (1994).
53. C. Vanderzande, *Lattice Models of Polymers* (Cambridge University Press, Cambridge, 1998).
54. V. Polyakov, *Zh. Eksp. Theor. Fiz.* **59**:542 (1970).
55. J. des Cloizeaux and Gerard Jannink, *Polymers in Solution* (Clarendon Press Oxford, 1990).
56. A. L. Owczarek (private communication).
57. P. Paule and M. Schorn, *J. Symb. Comp.* **20**:673 (1995).
58. M. T. Batchelor, *J. Phys. A* **26**:3733 (1993).
59. B. Duplantier and H. Saleur, *Phys. Rev. Lett.* **59**:539 (1987).
60. N. Read and H. Saleur, *Nucl. Phys. B* **613**:409 (2001), and references therein.
61. C. Tebaldi, M. De Menech, and A. L. Stella, *Phys. Rev. Lett.* **83**, 3952 (1999).
62. J. M. van den Broeck and L. W. Schwartz, *Siam J. Math. Anal.* **10**:639 (1979).
63. M. T. Batchelor, J. de Gier, and B. Nienhuis, *Int. J. Mod. Phys. B* **16**:1883 (2002).
64. N. M. Bogoliubov, A. V. Kitaev, and M. B. Zvonarev, *Phys. Rev. E* **65**:026126 (2002).
65. D. Zeilberger, *Electr. J. Combin.* **3**:R13 (1996).
66. G. Kuperberg, *Invent. Math. Res. Notes* **1996**:139 (1996).
67. V. E. Korepin, N. M. Bogoliubov, and A. G. Izergin, *Quantum Inverse Scattering Method and Correlation Functions*, (Cambridge University Press, Cambridge, 1993).